RSC Advances

ROYAL SOCIETY OF CHEMISTRY

www.rsc.org/advances

Journal Name

RSCPublishing

ARTICLE

$CuS-Bi_2S_3$ Hierarchical Architectures: Controlled Synthesis and Enhanced Visible-Light Photocatalytic Performance for Dye Degradation

Cite this: DOI: 10.1039/x0xx00000x

Received 00th January 2012,
Accepted 00th January 2012

DOI: 10.1039/x0xx00000x

www.rsc.org/

Lang Chen, Jie He, Qing Yuan, Yan-Wen Zhang, Fu Wang, Chak-Tong Au and Shuang-Feng Yin*

Novel $CuS-Bi_2S_3$ heterojunctions were fabricated by a one-step solvothermal method using glycol as solvent and L-lysine as structure-directing reagent. By varying the sulfur sources, $CuS-Bi_2S_3$ composites of different morphologies were obtained. Novel microspheres composed of ultrathin nanosheets and radial nanoneedles were synthesized using potassium thiocyanate (PT) and thiourea (TU) as sulfur sources, respectively. Based on the experimental and characterization results, we proposed a step-by-step mechanism for the growth of the $CuS-Bi_2S_3$ hierarchical architectures based on the different release rate of S^{2-} in the preparation process. It was observed that the $CuS-Bi_2S_3$ nancomposites show high photocatalytic activity for the degradation of dyes (Rh-B and CV, as well as both of them in an aqueous solution) under visible light ($\lambda \geq 400$ nm), showing performance much higher than those reported in the literatures. In terms of sulfur precursors, the degradation rates can be arranged the following order: TU>PT>ST>SS, and the optimal conditions for composite preparation are crystallization time of 6 h and Bi/Cu molar ratio of 10:1. The good photocatalytic activity is attributed to the matching of CuS and Bi_2S_3 band-gap energies as well as the CuS/Bi_2S_3 interfaces that facilitate transfer and separation of photogenerated charge carriers. With high stability, the $CuS-Bi_2S_3$ composites have high potential for the photodegradation of dyes in water-treatment processes.

Introduction

Controlled synthesis of visible-light photocatalysts (commonly made up of semiconductors) of unique morphologies is a popular research topic in the past decades. It is because the photocatalytic activity of semiconductors is dependent on their shape, structure, phase, size and crystal facets as well as the ways they are prepared.[1] Bismuth sulfide (Bi_2S_3) as an important V-VI semiconductor material is well studied for their potential applications in X-ray computed tomography imaging,[2] Schottky diodes,[3] lithium ion batteries,[4] gas sensors,[5] visible-wavelength photodetectors,[6] electrochemical hydrogen storage,[7] and hydrogen sensors.[8] In the past decades, Bi_2S_3 of different structures were synthesized. For example, high-quality Bi_2S_3 nanorods were prepared by a solvothermal method by Lou et al.[9] By means of aerosol-assisted chemical vapor deposition, Tahir et al. synthesized films of Bi_2S_3 nanoparticles and nanotubes that could be used as photoelectrodes.[10] By an acetylacetone solvothermal method, Zhou et al. synthesized Bi_2S_3 microspheres and microflowers that perform well in lithium ion batteries.[11] Yang et al. prepared Bi_2S_3 nanowires that function well as a thermoelectric material by a modified composite molten salt method.[12] Looking into the methods developed so far for Bi_2S_3 generation, one can see shortcomings such as the use of harmful solvents and additives as well as complication in synthesis. It is therefore interesting to develop methods that are simple, cost-effective, environment-benign and do not require harsh experimental conditions.

As a semiconductor with direct narrow band-gap (1.3-1.7 eV), Bi_2S_3 absorbs visible light ($\lambda \leq 800$ nm) and can be used as visible-light photocatalysts. Since the first report by Wu et al.[13] on the use of Bi_2S_3 nanodots and nanorods as photocatalysts for the degradation of dyes under UV light, this is much progress. Chen et al[14] reported a hierarchical structured Bi_2S_3 that functioned as photocatalyst for the decomposition of methyl orange under UV light. Luo et al[15] reported Bi_2S_3 nanorods for the degradation of Rh-B under visible light; despite it showed higher activity than Degussa P25, it took 4 h to reach complete Rh-B degradation under the adopted conditions (cat.: 50 mg, Rh-B: 10^{-5} mol/L×50 mL and 350 W Xe lamp). Over Bi_2S_3 dots, rods and sheets that are different in dominant facets, Huang et al[16] studied Rh-B photodegradation under visible light and reported that degradation efficiency could be related to surface dimensionality. It is observed that the time for complete removal of Rh-B is long (11 h) and catalyst recyclability is poor because of electrostatic interaction between dye molecules and catalyst. It is apparent that the photocatalytic performance of one-component Bi_2S_3 under UV or visible light is not satisfactory. This is attributed to the facile recombination of photogenerated electrons and holes due to the narrow bandgap between the conduction band (CB) and valance band (VB) of Bi_2S_3.

It is known that the presence of heterojunctions in a photocatalyst is beneficial for effective separation of charge carriers.[17] Liu et al. reported enhanced visible-light photocatalytic performance towards Rh-B degradation over

CuS-modified Bi_2S_3.[18] However, the photocatalytic activity under visible light is low and the reason for the enhanced activity remains unclear. In this paper, we report the synthesis of CuS-Bi_2S_3 micorspheres by a simple solvothermal method using glycol as solvent in the presence of L-lysine (a biomolecule used as structure-directing agent). The composites generated by this environment-benign process were evaluated for the photodegradation of Rh-B and crystal violet (CV) under visible light. Furthermore, we propose a step-by-step formation mechanism for controlled synthesis of the CuS-Bi_2S_3 composites as well as a mechanism to explain the enhancement of photocatalytic activity. We made estimation on the energy-band positions of Bi_2S_3 and CuS and deduced that the heterojunctions at the interfaces of CuS and Bi_2S_3 can prevent the recombination of photoexcited electrons and holes.

Experimental

Synthesis. The commercially available reagents were of analytical grade and were used without further purification. Typically, 10 mmol of $Bi(NO_3)_3{\cdot}5H_2O$ (4.85 g), 0.18 g of L-lysine and a proper amount of $CuCl_2$ were dissolved in 36 mL of glycol; the as-obtained transparent blue solution is named herein as solution A (the molar ratio of Bi to Cu were kept at 10:0.5, 10:1, 10:2, 10:4). Solution B was obtained by dissolving 0.18 g of L-lysine and a proper amount of sulfur source (i.e. thiourea (TU), sodium sulphide (SS), potassium thiocyanate (PT), sodium thiosulfate (ST)) in 36 mL of glycol. Then solution B was added dropwise into solution A under constant stirring. The resulted orange solution was transferred to a 100 mL Teflon-lined autoclave and maintained at 160 ºC for a designated period of time (3, 6 or 18 h). Then the autoclave with its content was cooled down to room temperature (RT) and the solid substance was collected by filtration, and washed several times with de-ionized water and absolute ethanol. After being dried in air at 80 ºC for 4 h, the samples were ready for use. Herein, the CuS-Bi_2S_3 composites with a Bi/Cu molar ratio of 10/1 prepared using sulfur source "X" and subject to solvothermally treatment of "y" hours is denoted as "X-yh". For example, the CuS-Bi_2S_3 composites with Bi/Cu molar ratio=10/1 prepared using TU, SS, PT, and ST as sulfur sources and subject to solvothermally treatment of 6 h are denoted as TU-6h, SS-6h, PT-6h, and ST-6h, respectively. As references, pure CuS and Bi_2S_3 samples were prepared using TU as sulfur sources (subject to 6 h of solvothermal treatment) but without the addition of $Bi(NO_3)_3{\cdot}5H_2O$ or $CuCl_2$, respectively.

Characterization. The as-prepared samples were characterized by powder X-ray diffraction (XRD) on a Bruker Automatic Diffractometer (Bruker D8 Advance) with monochromatized CuKα radiation (λ = 0.15406 nm) at a setting of 40 kV and 80 mA. The scanning rate was 0.02º (2θ)/s and the scanning range was 10-70º. X-ray photoelectron spectroscopy (XPS) was employed for the measurement of surface composition and chemical states of the CuS-Bi_2S_3 composites prepared using TU as sulfur source. The micro- and nano-structure as well as the morphology of as-prepared samples were examined using a field emission scanning electron microscope (FE-SEM) (Hitachi S-4800). Transmission electron microscopy (TEM) and high-resolution transmission electron microscopy (HRTEM) images were taken over a JEM-3010F transmission electron microscope at an accelerating voltage of 200 kV. The BET surface area was measured using a Quantachrome NovaWin instrument. UV-vis diffuse reflectance spectra (UV-vis DRS) were obtained over a UV-vis spectrophotometer (Cary 100) using $BaSO_4$ as reference material. Photoluminescence (PL) spectra were recorded using a Varia Cary Eclipse Fluorescence spectrophotometer at laser source of 425 nm.

Photocatalytic Activity. The photodegradation of Rh-B was employed to evaluate the photocatalytic activity of the as-prepared samples. Typically, 50 mg of catalyst was added into 100 mL aqueous solution of Rh-B (2.0×10^{-5} mol/L) in a Pyrex glass vessel. A 300 W Xe lamp was used to enable visible-light irradiation with a cut-off filter of λ≥400 nm. The distance between the light source and the surface of dye solution was kept at 25 cm and the light intensity was about 0.1 mW/cm^2. Before illumination, the suspension was stirred using a magnetic stirrer for 30 min in the dark to establish adsorption-desorption equilibrium between catalyst and dye. Then the mixture was exposed to visible light under constant stirring, and was sampled (about 3 mL) at designated intervals; with the removal of photocatalyst by centrifugation, the liquid was analyzed using a Cary-100 UV-vis spectrophotometer. The photocatalytic experiments were conducted at RT. Both the initial and final pH of the dye-containing solution (Rh-B, CV and their mixture) were in the range of 6.5-6.8. To demonstrate the wide application of the composite photocatalysts, CV (2.0×10^{-5} mol/L) and a mixture of Rh-B and CV (50 mL Rh-B solution and 50 mL CV solution, catalyst: 50 mg) were also studied under the same reaction conditions.

Results and discussion

Phase Structure. Shown in Figure 1 are the XRD patterns of Bi_2S_3, TU-3h, TU-6h and TU-18h. The pattern of as-synthesized Bi_2S_3 is ascribable to orthorhombic phase (JCPDS card No. 65-2431), whereas that of CuS to hexagonal phase (JCPDS card No. 06-0464). Besides displaying peaks similar to those of Bi_2S_3, the TU-3h, TU-6h and TU-18h samples show peaks at 2θ=27.9, 32.4, 46.4 and 54.9 due to CuS, indicating the successful preparation of CuS/Bi_2S_3 composites. In the cases of PT-3h, PT-6h and PT-18h, there is the detection of peaks corresponding to orthorhombic Bi_2S_3 and hexagonal CuS (see Figure S1, ESI, peaks belonging to CuS and Bi_2S_3 are marked by stars and triangles, respectively). It is noted that there is no significant change of XRD pattern upon the change of crystallization time across the PT-3h, PT-6h and PT-18h samples. With the addition of CuCl in the preparation process of Bi_2S_3, the diffraction peaks of Bi_2S_3 broaden (especially those between 20-35 degrees and 45-50 degrees), indicating the reduction of crystal size.

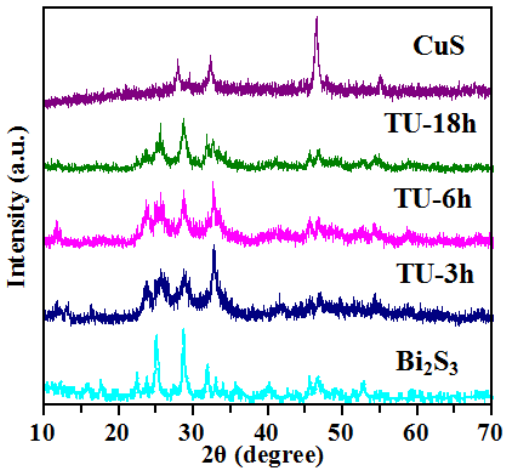

Figure 1. XRD patterns of CuS, Bi_2S_3, TU-3h, TU-6h and TU-18h

Surface Composition. To further study the composition of the composite samples, the TU-6h sample was analyzed by XPS with the peak positions calibrated against the C1s signal of contaminant carbon (binding energy = 284.6 eV). Figure 2(a) is a typical survey spectrum, showing the presence of Bi, Cu, S and a trace amount of C

and O. Figure 2(b) is the high-resolution Bi4f spectrum with two strong $Bi4f_{7/2}$ and $Bi4f_{5/2}$ peaks at 158.7 and 164.0 eV, respectively, which are characteristics of Bi^{3+}. The weak peaks located at 157.0 and 162.3 eV can be ascribed to the $Bi4f_{7/2}$ and $Bi4f_{5/2}$ signals of metal Bi, respectively,[19] whereas the weak peak located at 161.0 eV between the $Bi4f_{7/2}$ and $Bi4f_{5/2}$ peaks can be assigned to S2p signal.[20] Figure 2(c) displays the Cu 2p spectrum and the peaks at 931.9 and 952.0 eV are the $Cu2p_{3/2}$ and $Cu2p_{1/2}$ signals of CuS. The weak peak at 940.0 eV is a satellite peak.[21] Figure 2(d) shows S2s peak at 225.7 eV ascribable to S^{2-}. There is no detection of N1s signal (not shown here), confirming the complete removal of L-lysine and NO_3^-. The results of XPS analysis further confirm the presence of CuS and Bi_2S_3 in the composites.

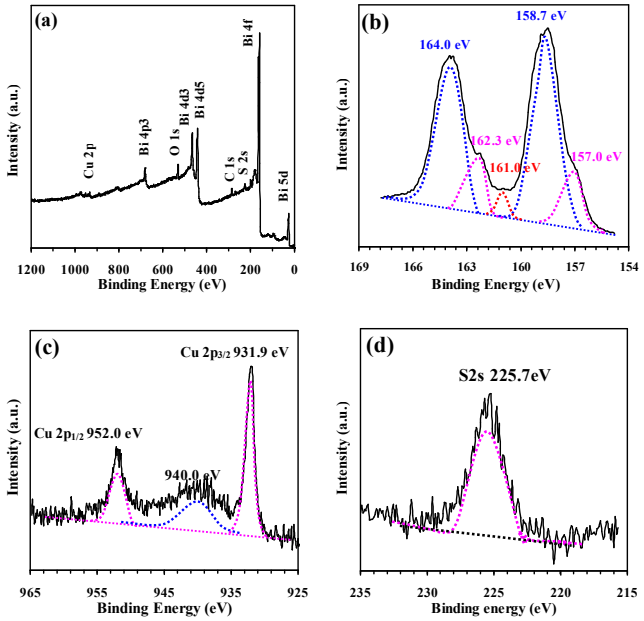

Figure 2. XPS spectra of TU-6h (a) survey, (b) Bi 4f, (c) Cu 2p, and (d) S 2s

Morphological Structure. The SEM images of CuS, Bi_2S_3 and TU-6h are displayed in Figure 3. One can see that the CuS sample is composed of irregular microspheres with diameters ranging from 500 nm to 4 μm. The microspheres are composed of nanoplates with nanoparticles dispersed on the surface (Figures 3(a) and (b)). Shown in Figures 3(c) and (d) are the low- and high-resolution SEM images of the Bi_2S_3 sample, and one can see cockscomb-like structures with diameter of 2-5 μm. As for the TU-6h sample, we observe uniform microspheres that are urchin-like with diameter of about 1.5 μm (Figure 3(e) and (f)). Compared to the size distributions of CuS and Bi_2S_3, that of CuS-Bi_2S_3 is much narrower. It was observed that the presence of CuS does not significantly affect the morphology of Bi_2S_3.

Effect of Sulfur Sources. In the synthesis of materials, it is often observed that factors such as precursor source and reaction condition have an influence on the physical and chemical properties of the final product.[22] Shown in Figure 4 are the SEM images of TU-6h, SS-6h, PT-6h, and ST-6h. The SS-6h sample is irregular in morphology, and is composed of nanoparticles and nanorods that are non-uniform in size (Figures 4(a) and (b)). The SEM image of ST-6h shows sheets that are 100 nm in thickness and 300-500 nm in width, and there is the dispersion of nanoparticles on the surface. To a certain extent, there is the assembly of sheets into the form of microspheres (Figures 4(c) and (d)). When PT and TU are used as sulfur sources, we obtained porous microspheres that are spongy-like and urchin-like. The former is about 800 nm in diameter and is composed of intertwining nanoplates (ca. 20 nm in thickness) (Figures 4(e) and (f)). The latter displays radial nanoneedles coming out from the sphere center (Figures 4(g) and (h)). The results of EDS analysis confirm the presence of Bi, Cu and S elements in the as-prepared samples (only those of PT-6h and TU-6h are given). The Cu-to-Bi molar ratio as indicated by the results of EDS and X-ray Fluorescence analyses (Figure 4(i)) are similar, and are in agreement with the theoretical value (i.e. 0.1).

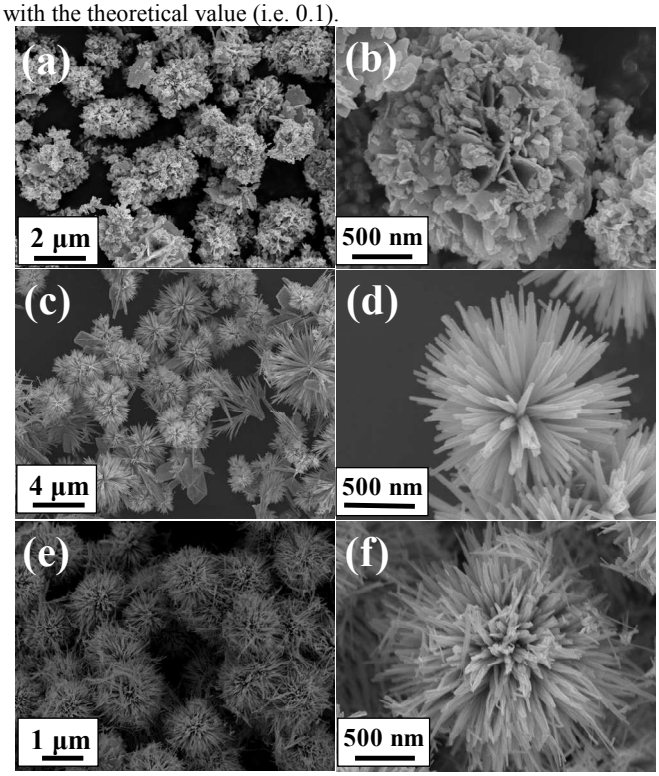

Figure 3. SEM images of (a)(b) CuS, (c)(d) Bi_2S_3 and (e)(f) TU-6h

Effect of Solvothermal Treatment Time. It is known that the crystallinity and morphology of nanomaterials are influenced by the time adopted for hydro- or solvo-thermal treatment. Despite the PT-3h, PT-6h and PT-18h samples show no apparent difference in phase structure and crystallinity (Figure S1, ESI), there is significant difference in terms of morphology. PT-3h is in the form of ultrathin nanoplates. One can find plates that are stacking together but there is no detection of regular pores between the plates, and there is no detection of microspheres (Figures 5(a) and (b)). When the thermal treatment is extended to 6 h (Figures 5(c) and (d)), one can see self-assembled spongy-like microspheres with diameter of about 800 nm. What is more, there is the existence of macropores known to be beneficial for the diffusion of reactants and products. Over PT-18h, one can see bigger microspheres (diameters ranging from 1 to 3 μm) with loose plates blocking some of the pore entrances (Figures 5(e) and (f)). Similar phenomena are also observed over the TU-3h, TU-6h and TU-18h samples. Shown in Figure S2 (ESI) are the time-dependent SEM images. At a growth time of 3 h, there is the appearance of nanoplates and nanoneedles. At 6 h, one can see uniform microspheres (about 1 μm in diameter) that are generated as a result of the self-assembly of nanoneedles, and there is no detection of nanoplates. At 18 h, the TU-18h sample displays larger microspheres (1 to 6 μm), showing nanoneedles longer than those of TU-6h. Based on the data, we consider that a solvothermal treatment period of 6 h is the most appropriate for the synthesis of the CuS-Bi_2S_3 nanocomposites.

The structure of PT-6h was further investigated using the TEM and HRTEM techniques. In consistent with the SEM results, the material is composed of ultrathin nanoplates as revealed in the low-

magnification TEM image (Figure 6(a)). Figure 6(b) is the HRTEM image of a selected area showing d-spacing of 0.183 nm, in agreement with that of (106) plane of Bi_2S_3, and the corresponding fast Fourier transform (FFT) pattern (Figure 6(c)) shows well-defined diffraction spots, indicating single crystallinity. Figure 6(d) is the HRTEM image of another selected area showing fringes of d=0.375 nm and d=0.326 nm which are in agreement with the (011) plane of Bi_2S_3 and (100) plane of CuS. It is clear that there are heterojunctions at the interfaces of Bi_2S_3 and CuS. The HRTEM images of samples prepared using TU and ST as sulfur sources further confirm the successful fabrication of CuS-Bi_2S_3 heterojunctions (Figure S3, ESI).

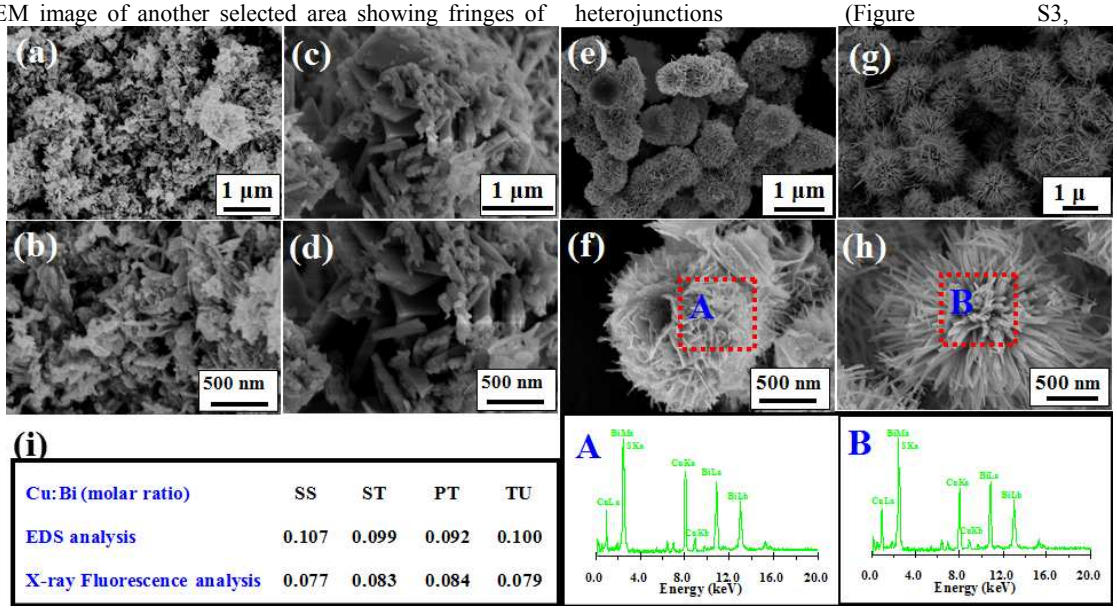

Figure 4. SEM images of (a)(b) SS-6h, (c)(d) ST-6h, (e)(f) PT-6h, (g)(h) TU-6h; (i) Cu-to-Bi molar ratios of composite samples as-indicated by EDS and X-ray Fluorescence analysis; A and B are the corresponding EDS patterns.

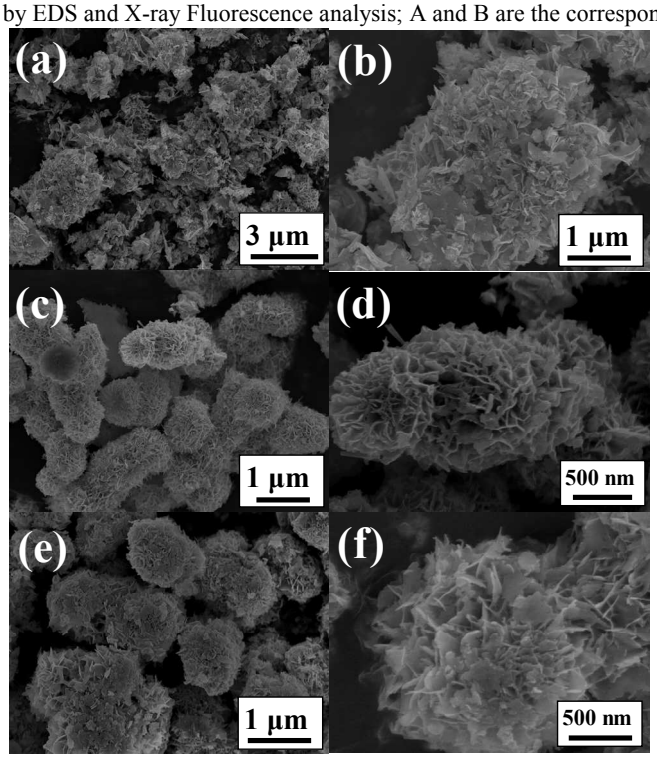

Figure 5. SEM images of (a)(b) PT-3h, (c)(d) PT-6h, and (e)(f) PT-18h

Possible Growth Mechanism. The specific surface area of three-dimensional microspheres with porous structures is much larger than that of the bulk counterparts. In other words, there is higher exposure of active sites with the former. For better design and synthesis of porous hierarchical materials, insight into the formation mechanism of CuS-Bi_2S_3 composites is beneficial. Based on the information accumulated in the present study, we propose a

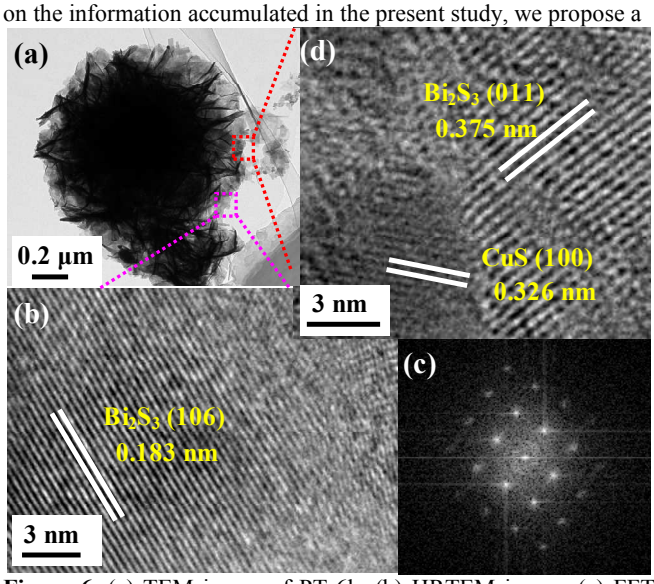

Figure 6. (a) TEM image of PT-6h, (b) HRTEM image, (c) FFT pattern, and (d) HRTEM image of selected area of PT-6h

plausible mechanism for the growth of the CuS-Bi_2S_3 hierarchical architectures (Figure S4, ESI). There is an immediate change of color from blue to orange when solution B (colorless) is added to solution A (blue). When the mixture are solvothermally treated at 160 ºC, the Bi^{3+} and Cu^{2+} in the solution react with S^{2-} at a rate that depends on how fast S^{2-} is released from the sulfur sources. The nucleation of CuS-Bi_2S_3 using SS as sulfur source is much faster than that using TU, PT or ST because there is the original presence of S^{2-} in the mixture. In the cases of using TU, PT or ST as sulfur source, the availability of S^{2-} is restricted by the partial dissociation of TU, PT or ST upon which there is the release of S^{2-}. When the

released S^{2-} reacts with Bi^{3+} and Cu^{2+}, there is the generation of CuS-Bi_2S_3 nuclei. With further release of S^{2-}, there is anisotropic growth of CuS-Bi_2S_3. Depending on the release rate of S^{2-}, there is the formation of CuS-Bi_2S_3 units that are different in size and/or shape. This phenomenon is quite similar to that observed in our previous work on the controlled synthesis of hollow and branched Bi_2O_3-Bi_2S_3 photocatalysts by an etching and re-growth method.[23] When TU, PT and ST are used as sulfur sources, units of nanoneedle, ultrathin nanoplate and thick sheet are generated, respectively. With the assistance of L-lysine, there is the self-assembly of units and finally the formation of the unique CuS-Bi_2S_3 composites.

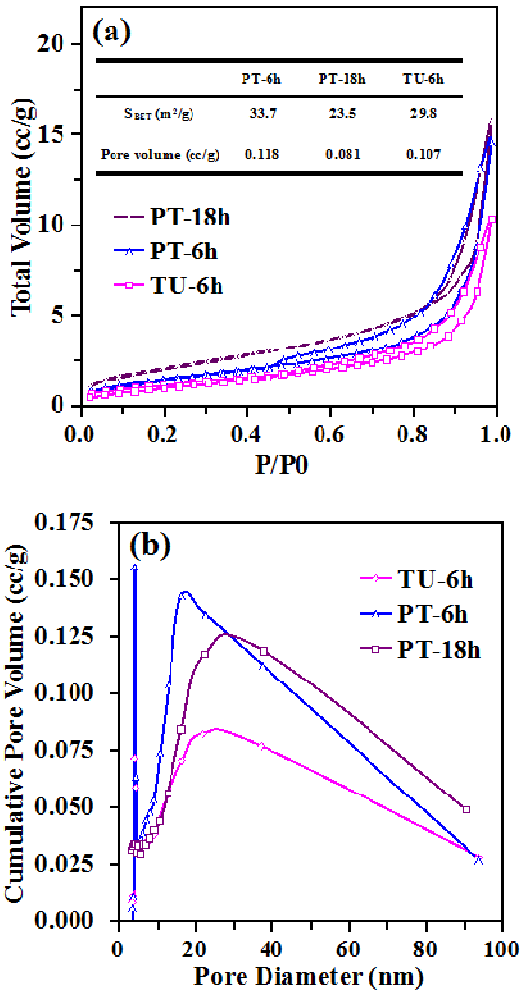

Figure 7. (a) Nitrogen adsorption-desorption isotherms, specific surface areas, and pore volumes, and (b) pore size distributions of PT-6h, PT-18h and TU-6h.

Nitrogen Adsorption-Desorption. Shown in Figure 7 are the isotherms of N_2 adsorption-desoprtion as well as the pore size distributions of the CuS-Bi_2S_3 composites. One can see that PT-6h and TU-6h show type-IV isotherms, and the hysteresis loops start at P/P_0=0.4 and show high adsorption at P/P_0=1.0, indicating the existence of mesopores and macropores. Over PT-18h, we observed type-IV isotherm with high adsorption at P_0=1.0, but the hysteresis loop starts at P/P_0=0.8, suggesting the presence of mesopores and macropores but absence of micropores (Figure 7(a)). The corresponding pore size distributions (estimated based on BJH method) shown in Figure 7(b) confirms the deduction. It is clear that there are micropores in PT-6h and TU-6h but not in PT-18h. The specific surface areas of PT-6h and PT-18h are 33.7 and 23.5 m^2/g, respectively. The total pore volumes of PT-6h, PT-18h and TU-6h are 0.118, 0.081 and 0.107 ml/g, respectively (inset of Figure 7(a)). The results of nitrogen adsorption-desorption analysis are in agreement with the SEM results that PT-6h, PT-18h and TU-6h are porous, and solvothermal treatment exceeding 6 h results in the loss of micropores. In other words, with the mature growth of microspheres, there is a decline in specific surface area and total pore volume.

Optical Properties. UV-visible diffuse reflectance spectra of PT-3h, PT-6h, PT-18h, ST-6h and TU-6h are displayed in Figure S5, (ESI). It is clear that all samples show absorption in both UV and visible-light regions. The absorption intensity increases with solvothermal treatment time plausibly due to crystallinity improvement. One can estimate the band gap of a semiconductor by plotting $(Ahv)^n$ vs (hv) using n=2 for direct transition semiconductors. The band gaps of CuS and Bi_2S_3 are 1.9 and 1.4 eV (Figure S6, ESI), respectively, in agreement with the values reported in the literature.[14,24]

The room-temperature photoluminescence (PL) emission was used to study the separation behavior of photogenerated charge carriers. It is known that a higher PL intensity implies lower efficiency of electron-hole separation.[17b,25] Illustrated in Figure 8 are the PL spectra of Bi_2S_3, TU-6h, TU-8h, TU-18h, PT-6h, and ST-6h. All composite samples show peaks similar to those of Bi_2S_3, but with much weaker peak intensity. Apparently, the PL intensity recorded over TU-6h is lower than that over TU-3h and TU-18h. On the other hand, the PL intensity recorded over ST-6h is higher than that over TU-6h and PT-6h. It is clear that for efficient separation of charge carriers, TU and PT are suitable sulfur sources, and a period of 6 h is appropriate for the solvothermal treatment.

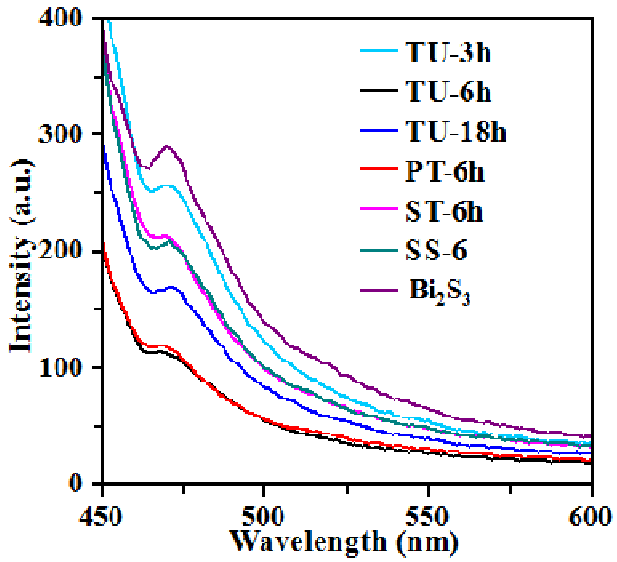

Figure 8. Room temperature PL spectra of TU-3h, TU-6h, TU-18h PT-6h and ST-6h (excited at 425 nm).

Photocatalytic Properties. Photocatalytic degradation of Rodamine-B (Rh-B) under visible light was used as a probe reaction to evaluate the activity of PT-3h, PT-8h and PT-18h, TU-6h and ST-6h (Figure 9). After the establishment of adsorption/desorption equilibrium in the dark, there is complete decolorization of Rh-B in 150 min over TU-6h (urchin-like) and PT-6h (porous spongy-like) microspheres, with the rate of the former higher than that of the latter. The adsorption of Rh-B on TU-6h, PT-6h, ST-6h, SS-6h, CuS and Bi2S3 are 64%, 60%, 40%,

32%, 1% and 18%, respectively. It is understood that the higher the adsorption of dyes on a photocatalyst the higher is the degradation rate. The Rh-B degradation rates over the composite samples prepared in this work are much higher than those over the ones prepared by a two-step method reported by Liu et al.[18] Despite the catalyst loading in the present study is only half of that adopted by Liu et al., the Rh-B degradation rate is 100% in 150 min whereas it was only 50% in 330 min in the case of Liu et al. Over ST-6h and SS-6h, the removal of Rh-B is 85% and 15% under the same conditions. We ascribe the high performance of TU-6h and PT-6h to their unique hierarchical structures. With sodium sulfide, the formation of composite is rapid, and its presence as nanoparticles and nanorods non-uniform in size is not beneficial to light harvesting, and hence the lower activity. As illustrated in the PL results (Figure 8), both the ultrathin nanoplates and nanoneedles are beneficial to prevent the recombination of photogenerated charge carriers. It is also observed that the CuS-Bi_2S_3 composites subject to solvothermal treatment of 6 h are high in photocatalytic activity (Figure S7, ESI), in agreement with the PL results.

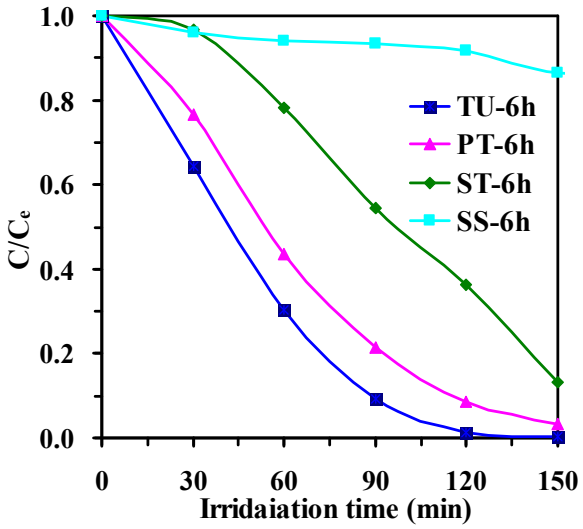

Figure 9. Photocatalytic degradation of Rh-B over PT-6h, TU-6h, SS-6h, and ST-6h

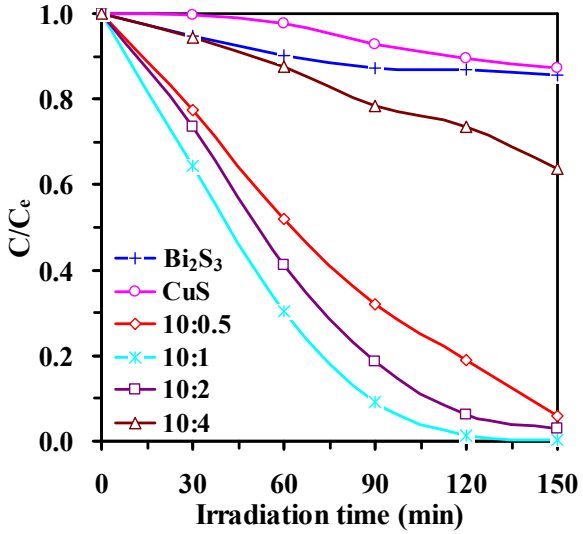

Figure 10. Effect of Bi/Cu molar ratio on the performance of CuS-Bi_2S_3 composites prepared using TU as sulfur source (solvothermally treated at 160 ºC for 6 h) in the photodegradation of Rh-B (2×10^{-5} mol/L).

The effect of Bi/Cu molar ratio on the photocatalytic activity was studied. It is clear from Figure 10 that the two-component CuS-Bi_2S_3 catalysts prepared using TU as sulfur source are higher than the one-component CuS and Bi_2S_3 catalysts in photocatalytic activity, and highest degradation rate is observed over the CuS-Bi_2S_3 catalyst with Bi/Cu molar ratio=10/1. The results suggest that at a Bi/Cu molar ratio of 10/1, there is the optimal formation of heterojunctions.

To assess the generality of the CuS-Bi_2S_3 catalysts, we evaluated the performance of PT-6h, TU-6h and Bi_2S_3 in the photodegradation of CV (known to be toxic to aquatic organisms) under the reaction conditions adopted for Rh-B degradation. One can see from Figures S8(a) and (b) (ESI) that there is 100% decolorization within 120 min over PT-6h and TU-6h whereas it is only 85% over Bi_2S_3 in a period of 180 min (Figure S8(c), ESI). The degradation rate constants further confirm that the composite samples show much higher photocatalytic activity towards different dyes than the single-component one (Table S1, ESI).

The performance of PT-6h was also evaluated when there is the co-presence of Rh-B and CV (50 mL Rh-B and 50 mL CV, both at a concentration of 2×10^{-5} mol/L). With irradiation time (Figure S9, ESI), the absorption peaks of Rh-B and CV decrease in intensity. The time required for the complete removal of dyes is about 210 min. The results confirm that PT-6h and TU-6h are efficient photocatalysts potentially applicable for dye removal from wastewater.

Possible Mechanism for Enhancement of Photocatalytic Activities. For semiconductors, the potentials of valance band (VB) and conduction band (CB) are calculated using the following empirical equations:

$$E_{VB}=X_{semconductor}(eV)-E^e+0.5\cdot E_g \quad (1)$$

$$E_{CB}=E_{VB}-E_g \quad (2)$$

$$X_{semconductor}(eV)=0.45\cdot X_{cation}(eV)+3.36 \quad (3)$$

$$X_{cation}(eV)=(X_{cation}(P.u.)+0.206)/0.336 \quad (4)$$

Where E_{VB} is the VB edge potential, $X_{semiconductor}(eV)$ is the semiconductor electronegativity, E^e is the energy of free electrons *vs.* hydrogen (4.5 eV), E_g is the band gap energy of semiconductor, E_{CB} is the CB edge potential, $X_{cation}(eV)$ is the absolute cationic electronegativity (eV) and $X_{cation}(P.u.)$ represents the cationic electonegativity (P.u. Pauling units).[26] The bandgap of CuS and Bi_2S_3 is found to be 1.9 and 1.4 eV, respectively. The VB and CB potentials of CuS and Bi_2S_3 as calculated using Eqs. (1)-(4) are adopted in Figure S10 that shows the band gap structures of CuS and Bi_2S_3 as well as the plausible processes for the separation of charge carriers. The CB potential of Bi_2S_3 is 0.08 eV, more negative than that of CuS (0.73 eV). There is hence diffusion of electrons through the heterojunctions from CB of Bi_2S_3 to CB of CuS. At the same time, there is transfer of holes from VB of CuS to VB of Bi_2S_3 because the VB potential of CuS is more positive than that of Bi_2S_3. Thus with the effective separation of charge carriers at the heterojunctions, there is enough time for the photogenerated electrons and holes to react with adsorbed OH^- and O_2, generating active ·OH and $\cdot O_2^-$ species for the degradation of dyes.

Conclusions

For the first time, CuS-Bi_2S_3 composites of unique hierarchical structures were synthesized by a one-step method using glycol as solvent in the presence of L-lysine. When thiourea and potassium thiocyanate are used as sulfur sources, there is the formation of urchin-like and porous spongy-like

microspheres, respectively; the former is composed of nanoneedles while the latter ultrathin nanoplates. The optimal thermal treatment conditions for their generation are Bi:Cu molar ratio of 10:1 at 160 ºC for 6 h. A growth mechanism that depends on the release rate of S^{2-} is proposed for the formation of the different morphologies. Compared to the single-component CuS and Bi_2S_3, the as-prepared two-component composites show much higher photocatalytic activity in the degradation of Rh-B and CV. The better performance is attributed to the hierarchical structures that enhance light absorption and generation of heterojunctions at the CuS/Bi_2S_3 interfaces. Based on the structures of CuS and Bi_2S_3 band gaps, it is deduced that there is enhanced transfer and separation of charge carriers at the heterojunctions. It is envisaged that the CuS-Bi_2S_3 photocatalysts are good candidates for the treatment of dyes-containing wastewater.

Acknowledgements

This project was financially supported by NSFC (Grant Nos. 21401054, 21476065 and J1210040), the China Postdoctoral Science Foundation (2014M562098) and the Fundamental Research Funds for the Central Universities. C. T. Au thanks the HNU for an adjunct professorship.

Notes and references

State Key Laboratory of Chemo/Biosensing and Chemometrics, College of Chemistry and Chemical Engineering, Hunan University, Changsha 410082, Hunan, People's Republic of China.
*Corresponding author: Phone: 86-731-88821171, Fax: 86-731-88821171, E-mail address: sf_yin@hnu.edu.cn
Electronic Supplementary Information (ESI) available: [XRD pattern, SEM, TEM(HRTEM) images, photocatalytic properties towards Rh-B, CV and composite dye degradation as well as the possible growth mechanism and charge carrier separation process]. See DOI: 10.1039/b000000x/

1 [a] S.Q. Liu, M.Q. Yang, Y.J. Xu, *J. Mater. Chem. A*, 2014, **2**, 430; [b] N. Tian, Z.Y. Zhou, S.G. Sun, Y. Ding, Z.L. Wang, *Science,* 2007, **316**, 732; [c] K.H. Reddy, S. Martha, K.M. Parida, *Inorg. Chem.,* 2013, **52**, 6390; [c] K. Zhang, J. Liang, S. Wang, J. Liu, K.X. Ren, X. Zheng, H. Luo, Y.J. Peng, X. Zou, X. Bo, J.H. Li, X.B. Yu, *Cryst. Growth Des.,* 2012, **12**, 793; [d] H.L. Xu, W.Z. Wang, *Angew. Chem. Int. Ed.,* 2007, **46**, 1489; [e] N. Roy, Y.K. Sohn, D. Pradhan, *ACS Nano,* 2013, **7**, 2532; [f] X. Wen, W.J. Luo, Z.G. Zou, *J. Mater. Chem. A*, 2013, **1**, 15479; [g] C.B. Xu, W.S. Yang, Q. Guo, D.X. Dai, M.D. Chen, X.M. Yang, *J. Am. Chem. Soc.,* 2013, **135**, 10206; [h] X.F. Li, X.Z. Zhen, S.G. Meng, J.J. Xian, Y. Shao, X.Z. Fu, D.Z. Li, *Envoron. Sci. Technol.,* 2013, **47**, 9911; [i] J.T. Han, Y.H. Huang, X.J. Wu, C.L. Wu, W. Wei, B. Peng, W. Huang, J.B. Goodenough, *Adv. Mater.,* 2006, **18**, 2145.
2 O. Rabin, J.M. Perez, J. Grimm, G. Wojtkiewicz, R.Weissleder, *Nat. Mater.,* 2006, **5**, 118.
3 H.F. Bao, C.M. Li, X.Q. Cui, Y. Gan, Q.L. Song, J. Guo, *Small,* 2008, **4**, 1125.
4 J.M. Ma, Z.F. Liu, J.B. Lian, X.C. Duan, T. Kim, P. Peng, X.D. Liu, Q. Chen, G. Yao, W.J. Zheng, *CrystEngComm,* 2011, **13**, 3072.
5 K. Yao, W.W. Gong, Y.F. Hu, X.L. Liang, Q. Chen, L.M. Peng, *J. Phys. Chem. C,* 2008, **112**, 8721.
6 [a] G. Konstantatos, L. Levina, J. Tang, E.H. Sargent, *Nano Lett.,* 2008, **8**, 4002; [b] X.L. Yu, C.B. Cao, *Cryst. Growth Des.,* 2008, **8**, 3951; [c] H. Bao, X. Cui, C.M. Li, Y. Gan, J. Zhang, J. Guo, *J. Phys. Chem. C,* 2007, **111**, 12279.
7 B. Zhang, X.C. Ye, W.Y. Hou, Y. Zhao, Y. Xie, *J Phys Chem B,* 2006, **110**, 8978.
8 K. Yao, W.W. Gong, Y.F. Hu, X.L. Liang, Q. Chen, L.M. Peng, *J Phys Chem C,* 2008, **112**, 8721.
9 W.J. Lou, M. Chen, X.B. Wang, W.M. Liu, *Chem. Mater.,* 2007, **19**, 872.
10 A.A. Tahir, M.A. Ehsan, M. Mazhar, K.G.U. Wijayantha, M. Zeller, A.D. Hunter, *Chem. Mater.,* 2010, **22**, 5084.
11 H.Y. Zhou, S.L. Xiong, L.Z. Wei, B.J. Xi, Y.C. Zhu, Y.T. Qian, *Cryst. Growth Des.,* 2009, **9**, 3862.
12 Q. Yang, C.G. Hu, S.X. Wang, Y. Xi, K.Y. Zhang, *J. Phys. Chem. C,* 2013, **117**, 5515.
13 T. Wu, X. Zhou, H. Zhang, X. Zhong, *Nano Res.,* 2010, **3**, 379.
14 F.J. Chen, Y.L. Cao, D.Z. Jia, *J. Colloid Inter. Sci.,* 2013, **404**, 110.
15 Y.F. Luo, H. Chen, X. Li, Z.Q. Gong, X.J. Wang, X.F. Peng, M.D. He, Z.Z. Sheng, *Mater. Lett.,* 2013, **105**, 12.
16 J. Huang, H. Zhang, X.G. Zhou, X.H. Zhong, *Mater. Chem. Phys.,* 2013, **138**, 755.
17 [a] L. Chen, S.F. Yin, S.L. Luo, R. Huang, Q. Zhang, T. Hong, C.T. Au, *Ind. Eng. Chem. Res.,* 2012, **51**, 6760; [b] L. Chen, Q. Zhang, R. Huang, S.F. Yin, S.L. Luo, C.T. Au, *Dalton Trans.,* 2012, **41**, 9513; [c] M. Xiong, L. Chen, R. Huang, Q. Yuan, J. He, S.L. Luo, C.T. Au, S.F. Yin, *Dalton Trans.*, 2014, **43**, 8331; [d] L. Chen, R. Huang, S.F. Yin, Y.J. Ma, Y.B. Zhou, S.L. Luo, C. T. Au, *RSC Adv.*, 2013, **3**, 24354; [e] Q. Yuan, L. Chen, M. Xiong, J. He, S.L. Luo, C.T. Au, S.F. Yin, *Chem. Eng. J.*, 2014, **255**, 3944 ; [f] S.G. Kumar, K.S.R.K. Rao, *RSC Adv.*, 2015, **5**, 3306..
18 Z.Q. Liu, W.Y. Huang, Y.M. Zhang, Y.X. Tong, *CrystEngComm,* 2012, **14**, 8261.
19 X.W. Liu, H.Q. Cao, J.F. Yin, *Nano Res.,* 2011, **4**, 470.
20 L. Tian, H.Y. Tan, J.J. Vittal, *Cryst. Growth Des.,* 2008, **8**, 734.
21 [a] J.G. Yu, J. Zhang, S.W. Liu, *J. Phys. Chem. C,* 2010, **114**, 13642; [b] J. Ghijsen, L.H. Tjeng, J.V. Elp, H. Eskes, J. Westerink, G.A. Sawatzky, M.T. Czyayk, *Phys. Rev. B*, 1988, **38**, 11322.
22 [a] H.F. Cheng, B.B. Huang, X.Y. Qin, X.Y. Zhang, Y. Dai, Chem Commun, 2012, **48**, 97; [b] Y.H. Ni, X.X. Wang, J.M. Hong, *RSC Adv.*, 2012, **2**, 546.
23 L. Chen, J. He, Q. Yuan, Y. Liu, C.T. Au, S.F. Yin, *J. Mater. Chem. A*, 2015, **3**, 1096.
24 X.Y. Meng, G.H. Tian, Y.J. Chen, R.T. Zhai, J. Zhou, Y.H. Shi, X.R. Cao, W. Zhou, H.G. Fu, *CrystEngComm,* 2013, **15**, 5144.
25 [a] H.F. Cheng, B.B. Huang, Y. Dai, X.Y. Qin, X.Y. Zhang, *Langmuir,* 2010, **26**, 6618; [b] C.L. Yu, K. Yang, J.C. Yu, F.F. Cao, X. Lin, X.C. Zhou, *J. Alloys Compd.,* 2011, **509**, 4547; [c] L. Chen, S.F. Yin, R. Huang, Q. Zhang, S.L. Luo, C.T. Au, *CrystEngComm,* 2012, **14**, 4217.
26 [a] L. Andrionic, L. Isac, A.J. Duta, *Photochem. Photobiol. A,* 2011, **221**, 30; [b] C.W. Kwon, A. Poquet, S. Mornet, G. Campet, M.H. Delville, M. Treguer, J. Portier, *Mater. Lett.,* 2001, **51**, 402.